Applied Energy 307 (2022) 118246

Contents lists available at ScienceDirect

Applied Energy

journal homepage: www.elsevier.com/locate/apenergy

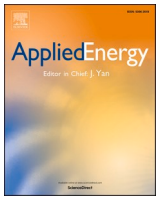

Hierarchical soft measurement of load current and state of charge for future smart lithium-ion batteries☆

Zhongbao Wei [a], Jian Hu [a], Yang Li [b], Hongwen He [a,*], Weihan Li [c], Dirk Uwe Sauer [c]

[a] National Engineering Laboratory for Electric Vehicles, School of Mechanical Engineering, Beijing Institute of Technology, Beijing, China
[b] Department of Electrical Engineering, Chalmers University of Technology, Sweden
[c] Chair for Electrochemical Energy Conversion and Storage Systems, Institute for Power Electronics and Electrical Drives (ISEA), RWTH Aachen University, Jaegerstrasse 17/19, 52066 Aachen, Germany

HIGHLIGHTS

- Hierarchy I method is a least squares-based moving horizon estimator.
- Hierarchy II method is a total least squares-based moving horizon estimator.
- Hierarchy III method is an input-free moving horizon estimator.
- Hierarchy II method is highly robust to the corruption of sensing noises.
- Hierarchy III method realizes accurate estimation without needing current sensor.

ARTICLE INFO

Keywords:
State of charge
Lithium-ion battery
Current sensor
Battery management
Input estimation

ABSTRACT

Accurate current measurement is indispensable for the management of lithium-ion battery (LIB), especially for the state-of-charge (SOC) estimation. However, accurate current sensing is challenging in electric vehicles (EVs) due to the electromagnetic interference. Moreover, the currents across the parallel branches of battery pack are even unmeasurable due to the absence of current sensor. Motivated by this, this paper proposes a hierarchical soft measurement framework for the load current and SOC addressing different degrees of current sensor uncertainty. Rooted from a common least squares (LS)-based state optimization problem, a total least square (TLS)-based modification is proposed and solved to compensate for the measurement disturbances, and in accordance to estimate the SOC more accurately. One step further, an input-free optimization method is proposed to co-estimate the SOC and load current without using the current measurements. Simulation and experimental results suggest that the proposed hierarchical framework can realize high-fidelity co-estimation of the SOC and load current, especially in the adverse scenarios of both strong noise corruption and current sensor malfunction/missing. The encouraging results open new paradigms for both the high-robustness current-free SOC estimation and the hardware-free soft current measurement of LIB.

1. Introduction

With the rapid development, the lithium-ion battery (LIB) has earned its popularity in power storage, electric vehicles (EVs), and portable electronics, attributed to its unique advantages of high energy/power density, long life span, and weak memory effects. As the performance of LIB system is principally determined by the weakest cells, the state-of-charge (SOC) that indicates the remaining charge of a cell is a critical state need to be monitored by the battery management system (BMS) to maintain the safe operation of LIB system [1–3].

SOC estimation has been widely explored in the past years, and the associated methods can be broadly divided into four categories, i.e., open circuit voltage (OCV) method, coulomb counting (CC) method, artificial intelligence method, and model-based method [4–6]. Except for the OCV method, it is well recognized that the rest approaches all depend directly on the accurate measurement of load current of battery.

☆ The short version of the paper was presented at ICAE2020, Dec 1–10, 2020. This paper is a substantial extension of the short version of the conference paper.

* Corresponding author.
E-mail address: hwhebit@bit.edu.cn (H. He).

https://doi.org/10.1016/j.apenergy.2021.118246
Received 30 April 2021; Received in revised form 19 November 2021; Accepted 20 November 2021
Available online 1 December 2021

Unfortunately, accurate current sensing could be quite challenging in practical EV applications. In the state-of-the-art techniques, the hall-effect current sensor and the shunt resistor current sensor are two major choices widely adopted for the BMS of EV [7]. Nevertheless, these techniques suffer from two recognized drawbacks for practical use. First, the current measurements contain remarkable errors due to the heavy electromagnetic interference and dynamic temperature condition within the EV environment. Second, the currents across parallel branches of the pack are not uniformly distributed due to cell inconsistency. It is not practical to install a physical current sensor for each parallel branch concerning the high cost. Such limitations have raised practical concerns and expectations for the BMS design, i.e., how to ensure the fidelity of SOC estimation with low-quality/noise-corruptive current measurement, or even without current sensors.

For the circumstance of low-quality current measurements, the exploration of novel current sensing techniques, e.g., on-chip temperature compensation and dynamic error-correction [8], can restore the measurement quality effectively. However, the installation of the complicatedly-structured sensor on each cell is not cost-friendly. Alternatively, the model-based SOC estimators have been most studied attribute to the high robust performance against disturbances. According to the specific model in use, such methods can be further categorized into electrochemical model-based [9–11] and equivalent circuit model (ECM)-based estimators [12]. On the premise of well-validated models, real-time SOC observers have been explored progressively, like Kalman Filter (KF) family [13–16], particle filter [17–19], H-infinity filter [20,21], sliding-mode observer [22], proportional integral-based observer [23], etc. Recent progresses have also transformed the SOC estimation into solving an optimization problem, which formulates the well-recognized moving horizon estimator (MHE) [24–26].

In spite of the successful use of existing model-based observers, their performance in practical scenarios can be deteriorated due to the difficulty in obtaining measurements with sufficient quality under special environmental constraints. Within this scope, low-quality sensing-induced biases of SOC estimation have been studied for most commonly-used EKF and least squares (LS) method in [27]. It is found that the sensor errors contribute to persistent estimation biases, and this contribution is in comparable magnitude to the model uncertainty. To remedy the impact of sensing noises, the wavelet transform has been employed to de-noise the corrupted measurements and thus to improve the accuracy of SOC estimation [28,29]. However, the low-frequency drifting errors are not likely to be eliminated by the filtering approaches. Moreover, the non-optimized filtering also risks distorting the original measurements if the parameters of filter are not tuned meticulously. Considering the current measurement offset (CMO), the two-stage recursive least squares algorithm has been exploited to deal with the interference of CMO on parameter identification and SOC estimation effectively [30].

In practical applications, more adverse conditions can occur where the current measurement is absolutely unavailable. A typical scenario is the occurrence of current sensor failure, while routine management tasks such as SOC estimation have to be ensured. Moreover, the refined LIB management requires the current flowing across each parallel-connected branch, which is typically not measurable due to the lack of physical sensors. To this end, few works that focus on the LIB management without using current sensor have been reported in the literature. Two current estimators based on a Thevenin model and a simple RC model are respectively proposed in [31,32]. The essence is to design a filter based on the transfer function of the battery model. In spite of the simplicity, the intrinsic open-loop mechanism inevitably results in low robustness to modeling and measurements uncertainty. A current unknown SOC estimation method is proposed by voltage filtering based on an ECM [33]. However, a primary model is utilized and the frequent relaxations are ignored, which potentially declines the estimation accuracy. To remedy such deficiencies, a closed-loop unknown input observer is proposed to estimate the SOC and input current concurrently based on a second-order RC model [34]. However, it is difficult to meet all the pre-conditions at the same time in practical applications.

To bridge the above research gap, this paper develops a hierarchical soft measurement framework for the SOC and load current, oriented for different degrees of current sensor uncertainty. In particular, the corresponding SOC estimation tasks are transformed into three optimization problems which are solved in a real-time manner with the MHE. Three primary contributions are made.

First, a hierarchical algorithmic framework is proposed, for the first time, to realize the accurate soft measurement of battery SOC and load current. The universal framework provides a series of estimators accounting for different degrees of current sensor uncertainties, i.e., accurate current measurement, heavily-corrupted current measurement, and no current measurement.

Second, the method from Hierarchy II can ensure high robustness against the disturbances on current measurements, including both drifting errors and stochastic noises. The accuracy of SOC estimate is improved largely compared to conventional methods in the heavy noise-corrupted condition.

Third, the method from Hierarchy III gives a solution for high-fidelity co-estimation of the input current and SOC without using the current sensor. This challenges the entrenched mindset that precise current measurements are imperative for accurate SOC estimation.

The remainder of the paper is organized as follows. The LIB modeling and parameterization are presented in Section 2. The proposed hierarchical soft-measurement framework is elaborated in Section 3. Simulation and experimental results are discussed in Sections 4 and 5, while the primary conclusions are drawn in Section 6.

2. Battery modelling

The high-fidelity objective modeling is the prerequisite for any model-based estimator or controller. A thorough exposition of the control-oriented models for the LIB can be found in [35]. A well-compromised model with sufficient simplicity yet simulating the dominant electrical dynamics of LIB is generally favorable for the formulated problem. To this end, the first-order RC model shown in Fig. 1 (a) is used in this paper, where the voltage source is used to simulate the SOC-dependent OCV, R_s is the ohmic resistance, the parallel connected R_p and C_p are polarization impedances describing the polarization effects of the LIB.

According to Kirchhoff's circuit laws and capacitor equation, the mathematical expression of the first-order RC model is expressed as:

$$C_p \frac{dV_p(t)}{dt} = I_L(t) - \frac{V_p(t)}{R_p} \tag{1a}$$

$$V_t(t) = V_{OC}(t) + I_L(t)R_s + V_p(t) \tag{1.b}$$

$$\frac{dz(t)}{dt} = \frac{\eta I_L(t)}{3600C_n} \tag{1c}$$

where I_L denotes the load current, z the battery SOC, C_n the nominal capacity (in Ah), V_p and V_t the polarization and terminal voltage, the OCV (V_{OC}) is a function of SOC:

$$V_{OC} = f(z) = \sum_{i=0}^{m} c_i z^i \tag{2}$$

where c_i are the coefficients, and m is the polynomial order.

The SOC-OCV test is performed and the commonly-used pulse-relaxation approach is used for calibrating Eq. (2) [36]. The curve-fitted SOC-OCV correlation is plotted against the experimental values in Fig. 1 (b), while the fitted coefficients are summarized in Table. 1.

Define the system input and output as I_L and $y_k = V_{t,k}$, the state as $\boldsymbol{x}_k = [V_{p,k}\ z_k]^{\boldsymbol{T}}$, the standard discrete-time state-space model can be determined from Eqs. (1.a)–(1.c) by:

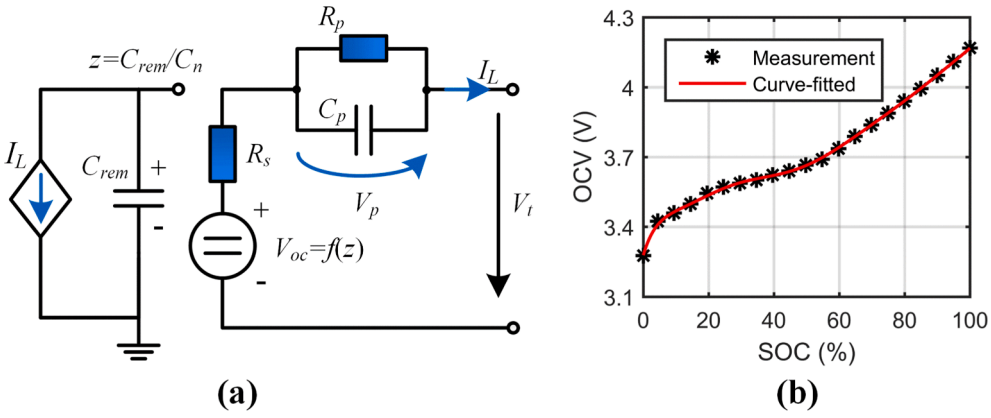

Fig. 1. First-order equivalent circuit model in use: (a) model structure, (b) SOC-OCV correlation.

Table 1
Coefficients of the SOC-OCV function.

Parameters	c_0	c_1	c_2	c_3	c_4
Value	3.301	2.176	−6.353	8.839	−3.805

$$\boldsymbol{x}_k = \boldsymbol{A}\boldsymbol{x}_{k-1} + \boldsymbol{B}I_{L,k-1} + w_k \tag{3a}$$

$$y_k = f(z_k) + V_{p,k} + R_s I_{L,k} + v_k \tag{3b}$$

where $\boldsymbol{w}_k$ and v_k are respectively the zero mean and Gaussian process and measurement disturbances, whose covariances are $\boldsymbol{Q}_k$ and R_k, respectively. V_{OC} is substituted by the relation between OCV and SOC $f(z_k)$ to interrelate the states with the system output. The reference matrices are given by:

$$\boldsymbol{A} = \begin{bmatrix} e^{-\frac{\Delta t}{R_p C_p}} & 0 \\ 0 & 1 \end{bmatrix}, \boldsymbol{B} = \begin{bmatrix} \left(1 - e^{-\frac{\Delta t}{R_p C_p}}\right) R_p & \frac{\Delta t}{C_n} \end{bmatrix}^T \tag{4}$$

The model parameters of the first-order RC model, i.e., R_s, R_p and C_p, are also SOC-dependent. Therefore, a hybrid pulse test is performed to calibrate these impedance parameters beforehand. Particularly, hybrid pulse sequences with charge/discharge pulses (10 s for each) and resting periods among them (40 s) are imposed on the LIB, and the impedance parameters of interest are offline identified with the obtained current–voltage responses. As the calibration method is a common one studied for years, the details are not elaborated herein but can be referred to the existing works [37].

3. Hierarchical estimation framework

In practical applications, current sensors can be contaminated by unignorable noises in heavy electromagnetic environments. Even worse, the current is unmeasurable in the parallel branches of the battery pack due to the difficulty of sensor installation. Regarding these two harsh conditions, this section goes further to elaborate a hierarchical co-estimation framework for SOC and input current based on the ECM presented in Section 2. In the proposed hierarchical framework, three constrained optimization problems are formulated, the solutions of which provide a series of estimation methods accounting for different degrees of current sensor uncertainties, i.e., accurate current measurement, heavily-corrupted current measurement, and no current measurement.

3.1. Hierarchy I: Conventional least squares-based problem formulation

To ease describing the proposed hierarchical algorithmic framework, a conventional optimization-based SOC estimation method is put forward in this section, as Hierarchy I of the proposed framework. Based on the general probability theory, it is well-recognized that the optimal estimation of internal states is a function of the conditional state probability density with knowledge of $\{\boldsymbol{y}_i\}k\ i = 0$ and system measurements, i.e., $\{\hat{\boldsymbol{x}}_i\}_{i=0}^{k} = F\left[\rho\left(\boldsymbol{x}_0, \ldots, \boldsymbol{x}_k | \boldsymbol{y}_0, \ldots, \boldsymbol{y}_k\right)\right]$. According to the Bayesian rule, this state estimation problem can be reformulated as a maximization task:

$$\{\hat{\boldsymbol{x}}_i\}_{i=0}^{k} = argmax\rho(\boldsymbol{x}_0, \ldots, \boldsymbol{x}_k | \boldsymbol{y}_0, \ldots, \boldsymbol{y}_k) \tag{5}$$

By combining the maximization problem of Eq. (5) with the state-space function of the ECM in Eqs. (3.a-b), a full information optimization for the battery states is given by [38]:

$$J\left(\{\hat{\boldsymbol{x}}_i\}_{i=0}^{k}\right) = argmin\|\boldsymbol{x}_0 - \hat{\boldsymbol{x}}_0\|_{P_0}^2 + \sum_{i=0}^{k} \left\|y_i - \left(f(\hat{z}_i) + \hat{V}_{p,i} + R_s I_{L,i}\right)\right\|_R^2 + \sum_{i=0}^{k-1} \left\|\hat{\boldsymbol{x}}_{i+1} - \boldsymbol{A}\hat{\boldsymbol{x}}_i - \boldsymbol{B}I_{L,i}\right\|_Q^2 \tag{6}$$

where $\boldsymbol{x}_0$ is the initial system state, P_0 is the initial state covariance used to penalize the deviation of the initial state estimate. Explicitly, the computational endeavor to solve the formulated optimization problem builds up rapidly with the enlargement of data length. This has motivated the exploration of the moving horizon framework which is believed to appeal to real-time embedded applications.

Suppose that a moving time horizon owning a fixed length of n is defined, then the k-th sampling can be divided into [0, …, t_{k-n}] and [t_{k-}

$_{n+1}$, …, t_k]. Bearing this in mind, the full information optimization problem of Eq. (6) can be reconstructed as:

$$J\left(\{\hat{\boldsymbol{x}}_i\}_{i=0}^{k}\right) = argmin\|\boldsymbol{x}_0 - \hat{\boldsymbol{x}}_0\|_{P_0}^2 + \sum_{i=0}^{k-n}\left\|y_i - \left(f(\hat{z}_i) + \hat{V}_{p,i} + R_s I_{L,i}\right)\right\|_R^2 + \sum_{i=0}^{k-n}\left\|\hat{\boldsymbol{x}}_{i+1} - \boldsymbol{A}\hat{\boldsymbol{x}}_i - \boldsymbol{B}I_{L,i}\right\|_Q^2 + \sum_{i=k-n+1}^{k}\left\|y_i - \left(f(\hat{z}_i) + \hat{V}_{p,i} + R_s I_{L,i}\right)\right\|_R^2 + \sum_{i=k-n+1}^{k-1}\left\|\hat{\boldsymbol{x}}_{i+1} - \boldsymbol{A}\hat{\boldsymbol{x}}_i - \boldsymbol{B}I_{L,i}\right\|_Q^2 \tag{7}$$

It is shown that the first three terms of Eq. (7) are meant to convey the historical information before the present time horizon, i.e., [0, …, t_{k-n}]. The first three terms are used to represent the arrival cost [39]. In accordance with this, the concerned state estimation problem at time t_k can be expressed as the following nonlinear optimization problem [24]:

$$\{\hat{\boldsymbol{\rho}}\}_{k-n}^{k-1} = \underset{\{\hat{\boldsymbol{\rho}}\}_{i=k-n}^{k-1}}{arg\ min}\left\{\begin{array}{l}\|\hat{\boldsymbol{x}}_{k-n+1} - \bar{\boldsymbol{x}}_{k-n}\|_{P_{k-n+1}}^2 + \sum_{i=k-n+1}^{k}\left\|I_{L,i}^m - \hat{I}_{L,i}\right\|_M^2 \\ + \sum_{i=k-n+1}^{k}\left\|y_i - \left(f(\hat{z}_i) + \hat{V}_{p,i} + R_s\hat{I}_{L,i}\right)\right\|_R^2\end{array}\right\} \tag{9a}$$

$$s.t.\quad 0 < z < 1 \tag{9b}$$

$$J\left(\{\hat{\boldsymbol{x}}_i\}_{i=0}^{k}\right) = argmin\|\boldsymbol{x}_{k-n+1} - \bar{\boldsymbol{x}}_{k-n+1}\|_{P_{k-n+1}}^2 + \sum_{i=k-n+1}^{k}\left\|y_i - \left(f(\hat{z}_i) + \hat{V}_{p,i} + R_s I_{L,i}\right)\right\|_R^2 + \sum_{i=k-n+1}^{k-1}\left\|\hat{\boldsymbol{x}}_{i+1} - \boldsymbol{A}\hat{\boldsymbol{x}}_i - \boldsymbol{B}I_{L,i}\right\|_Q^2 \tag{8}$$

where $\bar{\boldsymbol{x}}_{k-n+1}$ is the priori state estimate at the first of the time horizon, which is calculated by the $(k-n)$-th optimal estimate of states and the $(k-n+1)$-th system measurements. The first term represents the deviation of the initial state from the priori state estimate, and is called the arrival cost. The second term is the penalty accounting for the deviation between the measured and estimated terminal voltage calculated by the estimated SOC and V_p via the Eq. (3.b), and the third term is used to penalize the mismatch between the optimized estimated state and the propagated state via Eq. (3.a).

As the errors on the system input are not considered, the SOC estimation method based on Eq. (8) is called LS-MHE for simplicity. It is expected that the LS-MHE can give optimized estimation if the current measurements are free from errors. It is also worth noting that the LS-MHE has already been studied in the literature thus is not an innovation of this work. However, LS-MHE forms Hierarchy I of the proposed overall framework, since it lays the foundation for the methods in Hierarchy II and III, which are major contributions of this endeavor.

3.2. Hierarchy II: Total least squares-based problem formulation

The formulation of Eq. (8) gives a universal solution for the state estimation problem with accurate current measurements. However, as the current sensor is vulnerable to electromagnetic interference (EMI), precise current measurements are not always available in practical application, in contrast, the current measurements are usually contaminated by stochastic noises and drifting errors. In this regard, considering the current measurement errors, by introducing an extended vector $\boldsymbol{\rho} = [\boldsymbol{x}^T\ I_L]^T$, the total least squares (TLS)-based constrained optimization problem is formulated as:

$$\hat{\boldsymbol{x}}_k = \boldsymbol{A}\hat{\boldsymbol{x}}_{k-1} + \boldsymbol{B}\hat{I}_{L,k-1} \tag{9c}$$

$$y_k = f(z_k) + V_{p,k} + R_s\hat{I}_{L,k} \tag{9d}$$

$$\{\hat{\boldsymbol{\rho}}\}_{k-n}^{k-1} = \left[\hat{\boldsymbol{\rho}}_{k-n}^T \quad \hat{\boldsymbol{\rho}}_{k-n+1}^T \quad \cdots \quad \hat{\boldsymbol{\rho}}_{k-1}^T\right] \tag{9e}$$

$$\{\hat{\boldsymbol{x}}\}_{i=k-n}^{k-1} = \left[\hat{\boldsymbol{x}}_{k-n}^T \quad \hat{\boldsymbol{x}}_{k-n+1}^T \quad \cdots \quad \hat{\boldsymbol{x}}_{k-1}^T\right] \tag{9f}$$

where $I_{L,i}^m$ denotes the measured load current, $\sum_{i=k-n+1}^{k}\left\|I_{L,i}^m - \hat{I}_{L,i}\right\|_M^2$ is the input error term which is added into the objective function to form a TLS-based problem, M indicates the confidence on the current measurements, $\bar{\boldsymbol{x}}_{k-n+1}$ is updated with the estimate of input current at $k-n+1$. The SOC estimation method based on Eqs. (9. a - f) is called the TLS-MHE method for simplicity.

Unlike the problem formulation in Eq. (8), the proposed TLS-MHE method treats the system input as a decision variable to be estimated together with states of interest, using the state-space model as a constraint. Another primary difference is that the state error cost has been excluded referring to Eq. (8). This is reasonable with the assumption that the noise covariance $\boldsymbol{Q}$ is a zero matrix [40]. Hence, the state sequence is reconstructed via the process model once the initial state is optimized, which virtually decreases the solution time. By appropriately selecting the confidence factor M, the TLS-MHE method is supposed to accurately estimate the SOC and correct the load current measurements simultaneously. It is explicit that compared to the LS-MHE, the TLS-MHE has lower dependence on accurate current measurements, and is more robust to the disturbance on battery current. Therefore, the TLS-MHE method is expected to be favorable under the practical in-vehicle condition where the current measurements contain heavy noises.

3.3. Hierarchy III: Current-free constrained problem formulation

The aforementioned TLS-based method surmounts the challenge of

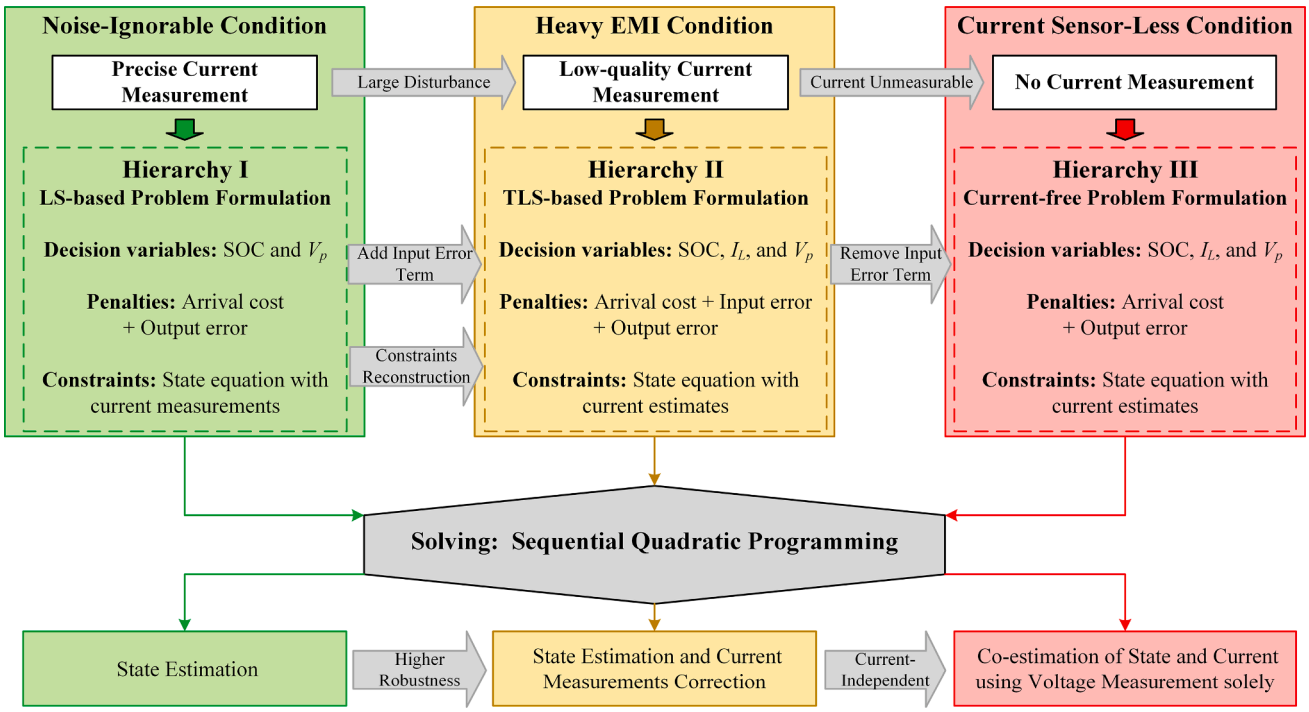

Fig. 2. Schematic diagram of the proposed hierarchical estimation framework.

SOC estimation with low-quality current measurements. However, in the current sensor-less scenario like the parallel topology in a battery pack, the current across each parallel branch is unmeasurable. In this circumstance, the input current is expected to be estimated simultaneously with the states of interest via matching the voltage measurements with the aid of the state-space model. In particular, a modified input-free optimization problem is formulated by:

$$\{\widehat{\boldsymbol{\rho}}\}_{k-n}^{k-1} = arg \min_{\{\widehat{\boldsymbol{\rho}}\}_{i=k-n}^{k-1}} \left\{ \begin{array}{c} \|\widehat{\boldsymbol{x}}_{k-n+1} - \bar{\boldsymbol{x}}_{k-n}\|_{P_{k-n+1}}^2 \\ + \sum_{i=k-n+1}^{k} \|y_i - \left(f(\widehat{z}_i) + \widehat{V}_{p,i} + R_s \widehat{I}_{L,i}\right)\|_R^2 \end{array} \right\} \tag{10}$$

It is worth noting that the constraints of Eq. (10) are consistent with those of the TLS-based method in Section 3.2. The main difference from the TLS-based method is the absence of input error term in the objective function, since the unavailability of current information is an underlying assumption herein. Note that the estimation at each time point relies only on the latest n terminal voltage measurements, while the historical measurements are readily contained in the arrival cost. By solving the finite-horizon optimization problem formulated in Eq. (10), both the states of interest and the input current can be estimated concurrently. As the estimation based on Eq. (10) no longer utilizes the current measurement, it is called current-free MHE for simplicity. Compared to the methods from Hierarchy I and II, the current-free MHE promises a unique advantage of estimation without a current sensor. This property appeals to some special scenarios like current sensor failure or the need for monitoring cells in the parallel branches of the pack.

3.4. Universal framework of the hierarchical methodology

The efficient solution of constrained optimization problems defined in Sections 3.1–3.3 eventually gives rise to a series of estimation methods accounting for different degrees of current sensor uncertainties. In this paper, the sequential quadratic programming (SQP) method is employed to solve the involved optimization problems and thus provide the optimal estimates of SOC and input current at each iteration. For the sake of simplicity, the algorithmic procedure of the SQP is not detailed in this paper but can be found in [41].

The proposed hierarchical framework is shown schematically in Fig. 2. It can be seen that one can always find a solution in response to different levels of current sensor uncertainty. In particular, the conventional LS-MHE represents “Hierarchy I”, which is preferable for use

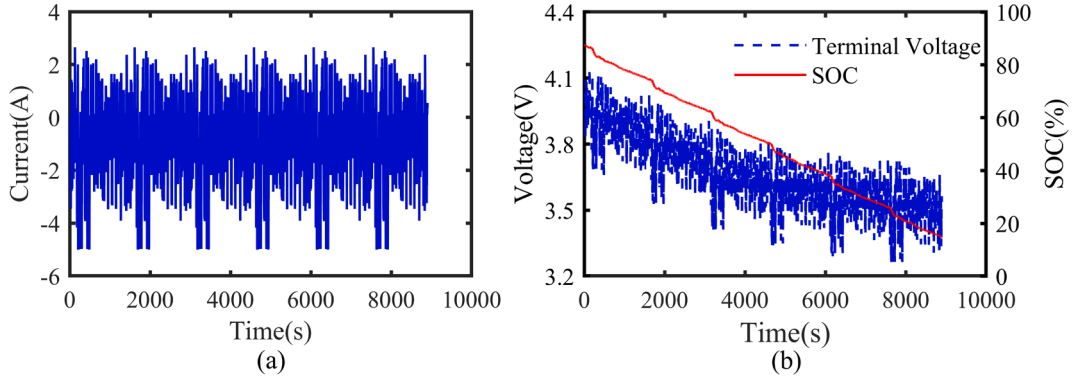

Fig. 3. Profiles of load current, terminal voltage and SOC for simulation study: (a) FUDS current, and (b) terminal voltage and reference SOC.

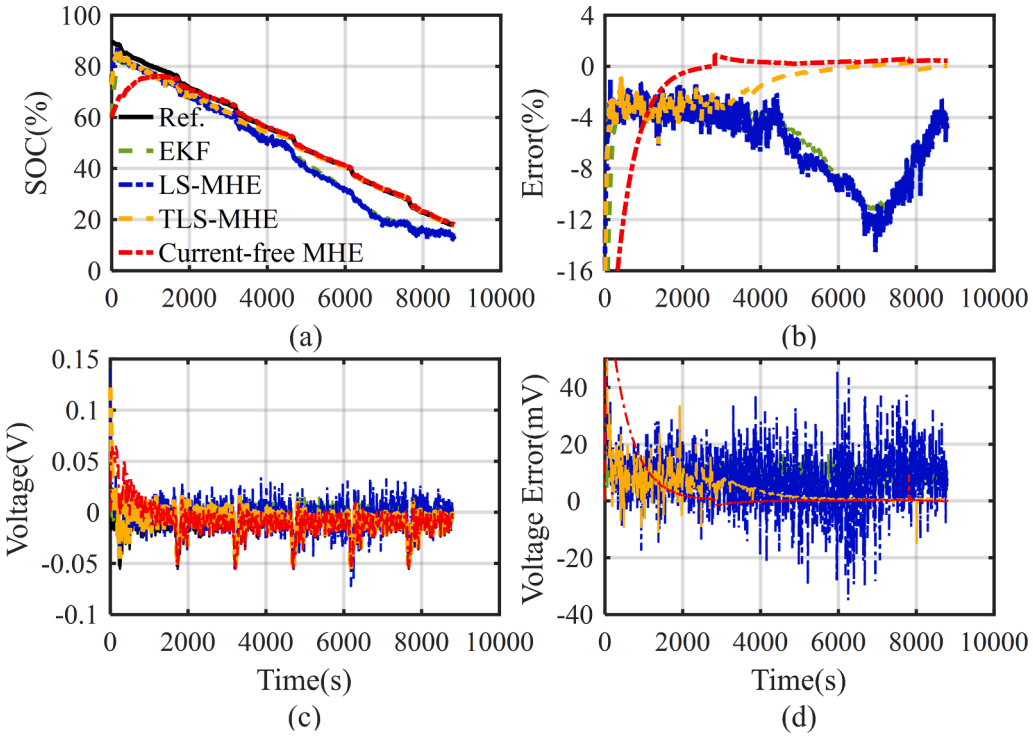

Fig. 4. State estimation results of simulation study: (a) estimates of SOC, (b) SOC estimation error, (c) estimates of polarization voltage, (d) estimation error of polarization voltage.

Table 2
Comparative estimation performance of different methods obtained from simulation I.

Methods	SOC (%)		V_p (mV)		Input current (A)	
	MAE	RMSE	MAE	RMSE	MAE	RMSE
EKF	5.43	6.11	9.9	10.1	N.A.	N.A.
LS-MHE	5.99	6.69	9.1	10.9	N.A	N.A
TLS-MHE	1.49	2.03	3.9	5.7	0.215	0.298
Current-free MHE	0.61	0.97	3.3	4.9	0.072	0.135

under a favorable condition that the LIB current can be measured very precisely.

In "Hierarchy II", the TLS-MHE is employed to estimate the SOC and correct the current measurements concurrently. It is worth noting that the current measurements are subjected to heavy noises and drifting errors due to the dynamic working condition and electromagnetic interference of in-vehicle environment. Affected by these uncertainties, the existing estimation methods are easily deteriorated in the estimation accuracy. In contrast, this method mitigates the reliance on highly-precise measurement, and thus appeals to a deteriorated condition that the current and voltage measurements of LIB are low-quality with large disturbances.

In "Hierarchy", the proposed current-free MHE eliminates completely the dependence on the current measurements by co-estimating the SOC and load current using only the voltage measurements. This indicates its suitability for use under the most deteriorative scenario, where the current of LIB is not measurable due to either sensor breakdown or the difficulty of large-scale sensor installation.

4. Simulation validation

The performance of the proposed framework in comparison with existing ones in the literature is evaluated with simulations in this section. The merit of simulation is rooted in the full elimination of model uncertainty, which enables evaluating the algorithms from a purely theoretical perspective.

4.1. Data acquisition

During the simulation, the federal urban drive schedule (FUDS) is loaded to excite the battery model, while the load current, terminal voltage and SOC are sampled at 1 Hz and plotted in Fig. 3. The methods are performed with the acquired data to evaluate the effectiveness. The widely-used EKF-based state estimator is also executed and compared with the proposed methods to evaluate the performance of different methods. Since the precise initial SOC is unavailable practical applications, the SOC is initialized erroneously as 60% in this work, while the true initial SOC is 87.5%.

4.2. Simulation results

Random noises with a standard deviation of 0.5 A (10% when normalized by the range of the FUDS current) and 2 mV, as well as drifting errors of 0.5 A and 2 mV are added to the noise-free current and voltage measurements to simulate the scenario with heavy EMI. Note that the voltage disturbances are much smaller because the commercial voltage sensors of BMS can generally ensure a much higher precision than the current measurement. The estimation results by using the proposed framework, including the LS-MHE (Hierarchy I), TLS-MHE (Hierarchy II), and current-free MHE (Hierarchy) are plotted in Fig. 4. Meanwhile, the estimation results given by the widely-used EKF are also plotted against the ones from the hierarchical framework for a straightforward comparison. The corresponding MAEs and RMSEs of state estimation after the algorithms converge to within ± 5% error bound are summarized in Table 2.

As shown in Fig. 4 (a-b) and Table 2, the SOC estimates with EKF and LS-MHE are comparable, and both of them suffer from a major error build-up due to the addition of large measurement errors. The estimation errors of these two methods keep around 4% in the first 4000 s and reach the maximum of 14 % at around 7000 s. The low robustness of LS-

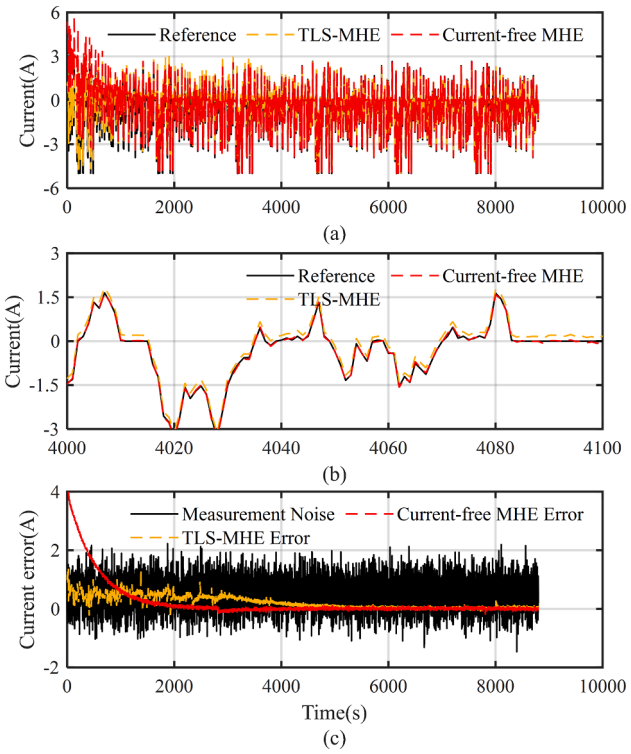

Fig. 5. Estimated input current of simulation study: (a) input current estimates, (b) partial zoom-in figure.

MHE (Hierarchy I) can be explained by the optimization problem formulation in Eq. (8), which assumes a disturbance-free system input (load current measurement). In reality however, this deviation from such assumption virtually leads to a deteriorative performance of LS-MHE. Even worse, the regional flat SOC-OCV curve within the SOC range of 20–50% causes a quasi-unobservable condition and thus a growing vulnerability to perturbations. As the disturbances imposed on the current and voltage data are eventually transferred into the estimated OCV, the enlarged SOC mismatch is hence within expectation for these two methods.

In contrast, it is shown that the estimation errors of TLS-MHE (Hierarchy II) are much lower and always kept within the ±4% error bound. The superior performance of TLS-MHE is attributed to its full consideration of the disturbances on both current and voltage measurement, as suggested by Eq. (9), and the "error-in-variable" optimization mechanism can well compensate for such disturbances to ensure an unbiased estimation. Moreover, the TLS-MHE converges into the 4% error bounds rapidly in the first tens of seconds. The observed fast convergence is attributed to the input error penalty in objective function Eq. (9), where the estimation is guided efficiently towards the "correct direction" with the low-quality current measurements, but does not fully trust the measurements. With respect to the current-free MHE (Hierarchy), its estimate of SOC converges into the 4% error bounds gradually in nearly 1000 s and keeps tracking of the benchmarked SOC trajectory closely. The relatively slow convergence of the current-free MHE can be explained from two perspective. On the one hand, as the input current is added into the decision variables, the elevated degree of freedom of the current-free MHE make the optimization more complex. On the other hand, the weight of the arrival cost in the objective function grows significantly as the input error term is removed, which limits the

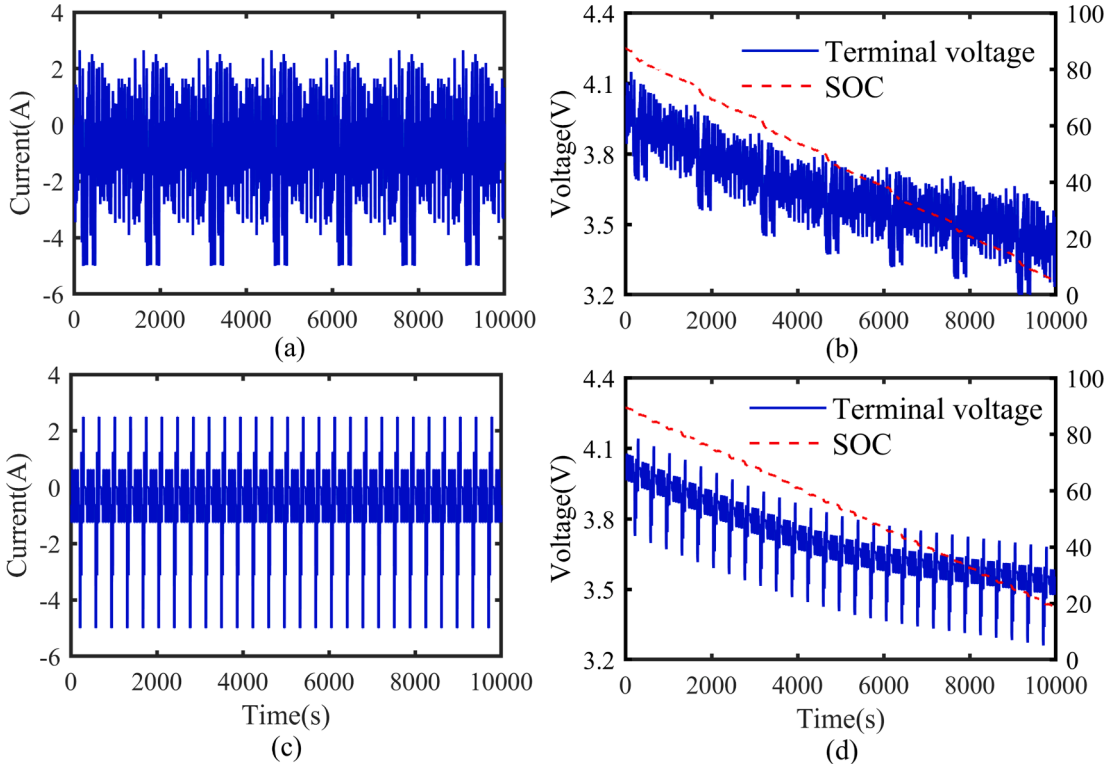

Fig. 6. Data from experiments: (a) input current, and (b) terminal voltage and benchmarked SOC under FUDS, (c) input current, and (d) terminal voltage and benchmarked SOC under DST.

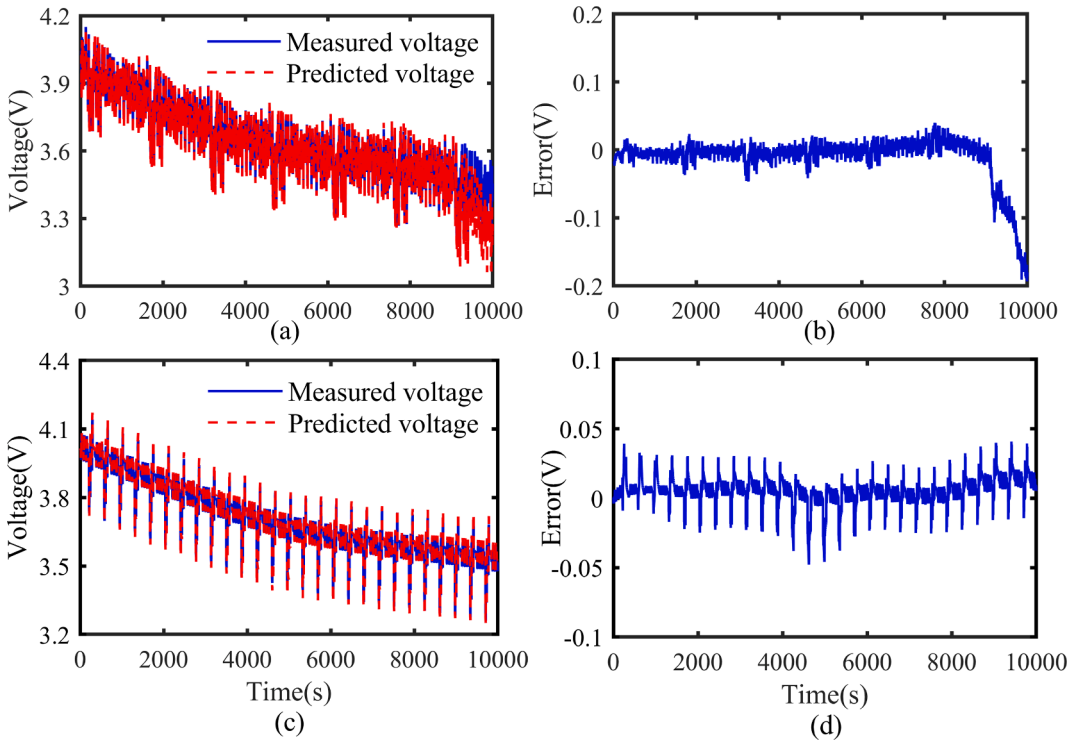

Fig. 7. Modelling results: (a) predicted terminal voltages against measurements and (b) modelling error under FUDS, (c) predicted terminal voltages against measurements and (d) modelling error under DST.

propagation step size of the SOC estimates at each iteration. As shown in Table 2, the steady-state estimation deviation is even lower than the TLS-MHE, which can be explained by the fact that the method is independent of the current measurement, so that the errors cannot be transferred to the state estimation.

The estimation of polarization voltage, which is cross-linked with the SOC estimation, can serve as an important support for the aforementioned discussions. As can be seen in Fig. 4 (c-d), the results are consistent with those of SOC estimation for all the four involved methods. Therefore, this is not expanded for discussion for the briefness.

It is worth noting that both the TLS-MHE and the current-free MHE can achieve input current estimation, although the former needs a rough measurement as the basis. The estimation results of the input current by using the two methods are shown in Fig. 5, while the statistical indicators are summarized in the last columns of Table 2. It is observed that both the estimates agree with the ground truth closely. The scrutiny

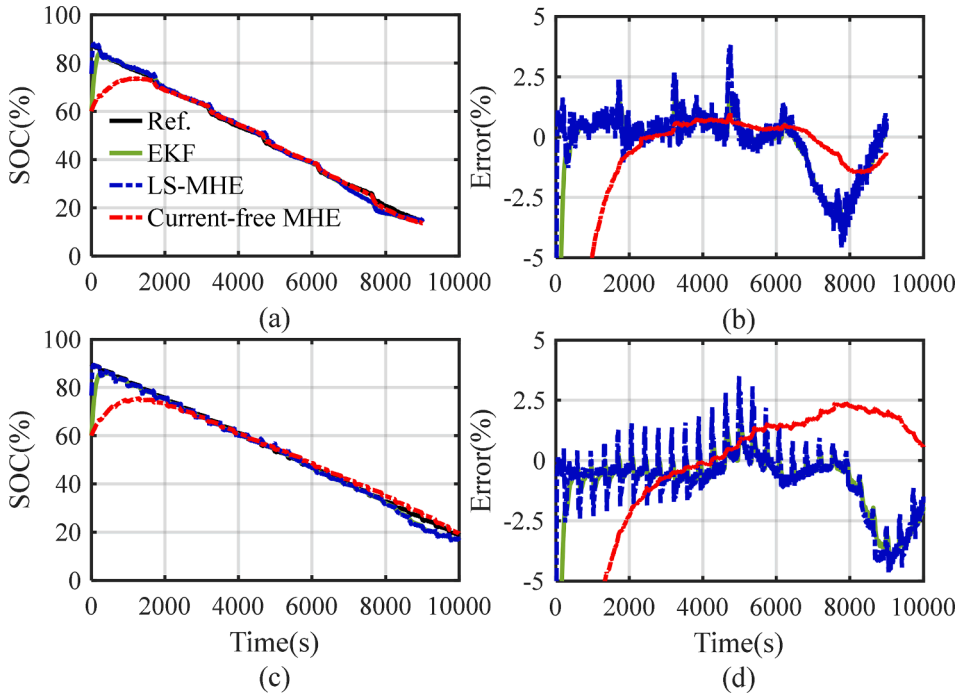

Fig. 8. SOC estimation results under ignorable noise corruption: (a-b) SOC estimates under FUDS, (c-d) SOC estimates under DST.

Table 3
Estimation error of SOC under ignorable noise corruption.

	FUDS		DST	
	MAE	RMSE	MAE	RMSE
EKF	0.85%	1.26%	0.99%	1.42%
LS-MHE	0.890%	1.31%	1.01%	1.54%
Current-free MHE	0.781%	1.11%	1.45%	1.71%

of estimation errors, as shown in Fig. 5 (b, c), reveals that the two methods mitigate most of the noises and offset imposed on the current measurements. By comparison, the current-free MHE gives rise to an even more accurate steady-state estimation of the input current, even though it absolutely eliminates the need for current sensing.

A potential limitation of the current-free MHE is the slower convergence during the start-up stage compared to the TLS-MHE, as supported by Fig. 4 (a-b) and Fig. 5 (c). In spite of this, the current-free MHE outperforms the methods in other hierarchies from the viewpoint that, it is applicable with expected performance without the need for current sensor installation. This unique merit appeals for wider applications including some special scenarios, such as the case of current sensor failure or the need for monitoring cells in the parallel branches of the pack.

5. Experimental validation and discussion

5.1. Experimental details

The algorithms are evaluated experimentally using both the FUDS and the DST condition in this section. Arbin battery testing system is used to load the dynamic current profiles to the LIB in use. The ranges of the current and voltage sensors inside the test bench are 10 A and 5 V, while the measurement error limits are both within 0.05%. The acquired high-accuracy experimental data including the load current and terminal voltage are collected at 1 Hz and used to obtain the benchmarked SOC trajectory, which is used to evaluate the performance of different methods. Particularly, the reference SOC trajectory is determined by combining the accurate SOC pre-setting and CC-based calibration. The measurements and the benchmarked SOC trajectory are shown in Fig. 6.

Table 4
Errors of input current estimation under ignorable noise corruption.

	FUDS	DST
MAE	0.137 A	0.151 A
RMSE	0.178 A	0.197 A

5.2. Validation of modelling accuracy

The modeled terminal voltages are plotted against the measured values in Fig. 7. It is shown that the modeled terminal voltages approach their measurements very tightly. The modeling errors have been confined to the 50 mV error bound for both of the two validating conditions, except for a visually observable error build-up at the ending stage of the FUDS condition. This is caused by the high nonlinearity of LIB dynamics at the low SOC region (typically lower than 15%), which can be hardly described by the first-order RC model employed in this paper. Fortunately, such deep charge depletion is hardly met in practice as a consequence of the intention to protect the battery. It is hence validated the parameterized model is highly authentic to describe the LIB electrical dynamics, offering a solid basis for the model-based state and input current co-estimation.

5.3. Experimental validation with ignorable noise corruption

Measurements with high-precision sensors under well-protected laboratory conditions are used for method validation herein. With high-fidelity measurements, the TLS-MHE is approximately equivalent to the LS-MHE. Hence, only the LS-MHE, current-free MHE, and the widely-used EKF are included for comparison in this section.

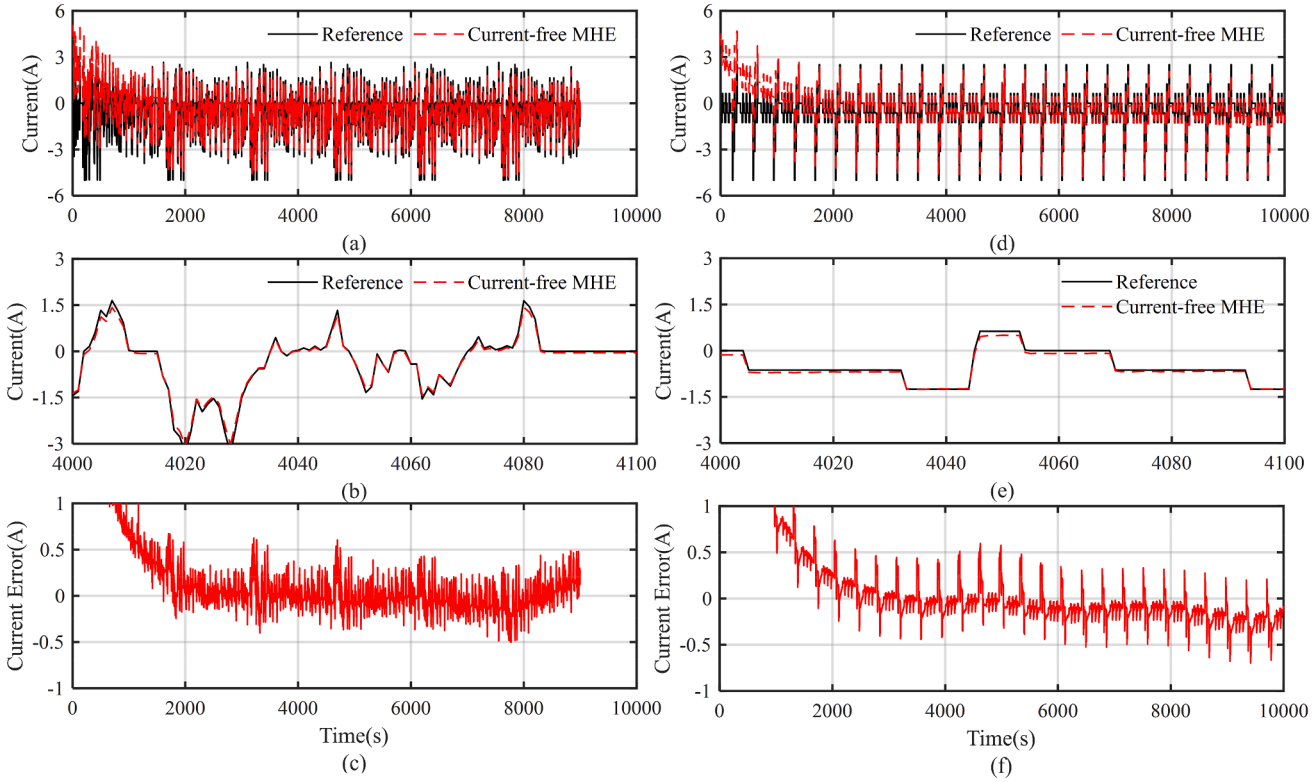

Fig. 9. Results of input current estimation under ignorable noise corruption: (a-c) estimation under FUDS, (d-f) estimation under DST.

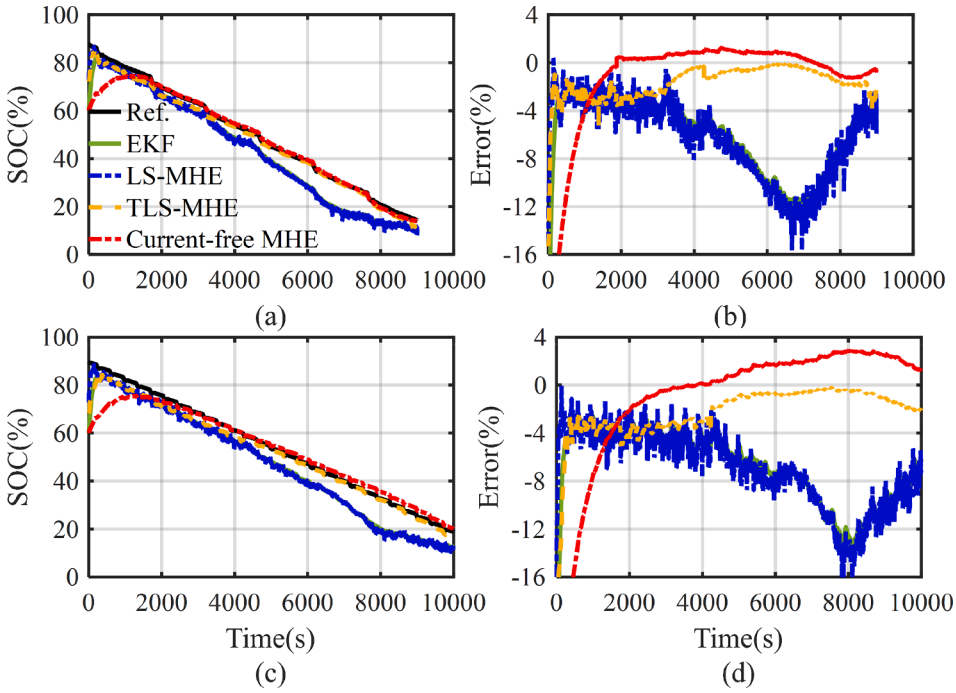

Fig. 10. SOC estimation results with heavy disturbances: estimates and errors under (a-b) FUDS, and (c-d) DST.

Table 5
SOC estimation errors with heavy disturbances.

	FUDS		DST	
	MAE	RMSE	MAE	RMSE
EKF	5.75%	6.52%	6.40%	7.07%
LS-MHE	6.22%	7.05%	6.97%	7.66%
TLS-MHE	1.59%	1.92%	1.99%	2.42%
Current-free MHE	0.87%	1.11%	1.67%	1.95%

The results of the SOC estimation under FUDS and DST conditions are illustrated in Fig. 8, and correspondingly, the statistical results of estimation deviation (MAE and RMSE) in the steady-state are summarized in Table. 3. It is shown that the widely-used EKF and LS-MHE (Hierarchy I) can estimate the SOC accurately. This is within expectation since the algorithms are implemented in an environment with ignorable noise corruption. By comparison, the proposed current-free MHE method augments the input current to the state space for co-estimation, which risks declining the estimation performance due to the elevated degrees of freedom and the incurred cross-interference problem. This problem indeed exists, witnessed by the slow convergence at the initial stage. Once converged, however, the current-free MHE exhibits an equivalent accuracy compared to the benchmarked EKF and LS-MHE which utilize the high-quality input current information.

By using the current-free MHE, the estimation results of input current are shown in Fig. 9 (a-c, d-f) in comparison with their benchmarks measured by the high-precision sensors. In correspondence to the convergence of SOC estimation, it takes a transition period for the current-free MHE method to alleviate the initialization error. After this stage, the input current estimates track the noise-free current measurements reference closely. Despite that the maximum estimation error that appears at the transient change of the current is nearly 0.6 A, the average estimation error is within a reasonable range under both the FUDS and DST conditions. This can be justified by the statistical error information summarized in Table. 4. The estimation RMSEs are 0.151 A and 0.197 A under the two conditions, respectively. The normalized RMSEs are smaller than 4%, which stands for a high accuracy considering the same level of precision of Hall-effect current sensors which are widely used.

Two major conclusions can be drawn from the experimental results in this section. First, under the scenario of ignorable or slight noise corruption, the LS-MHE provides sufficient estimation performance that similar to the EKF. There is no need to move to hierarchy II or III, which inevitably increases the computing complexity. Second, the current-free MHE method is capable of co-estimation of the battery input current profile and SOC with sufficient accuracy leveraging merely the voltage measurements.

5.4. *Experimental validation with heavy disturbance*

In this section, remarkable disturbances consistent with the simulation study are imposed on the current and terminal voltage measurements. The SOC estimation results of the EKF, LS-MHE, TLS-MHE, current-free MHE methods are plotted in Fig. 10, and the statistical errors are summarized in Table. 5.

It can be observed that the SOC estimation results by using EKF and LS-MHE methods are similar to the simulation study. Although all the methods converge stably and track the reference closely, the accuracy has declined compared to the case of simulation due to the existence of modeling uncertainties. Referring to Table. 5, the SOC estimates with EKF and LS-MHE show large errors thus are no longer recommended for use in practice. By comparison, the TLS-MHE and current-free MHE can remedy this deficiency. It is observed that the estimation results of these two methods keep high accuracy within the heavy noise-corruptive scenario. As discussed in Section 4.2, TLS-MHE attenuates the effect of disturbances by augmenting the input error penalty into the objective function, while the current-free MHE completely rules out the reliance on the noise-corrupted current information. Therefore, the disturbance-tolerant property of the two methods can be explained. Consistent with the simulation results, the current-free MHE shows a higher steady-state accuracy but a deteriorated converging performance. Both of them (Hierarchy II and III) are applicable with sufficient precision under the adverse but practical in-vehicle condition of heavy noise corruption. In the case that the current measurements are not available, the current-free MHE (Hierarchy III) can be used for high-fidelity SOC estimation.

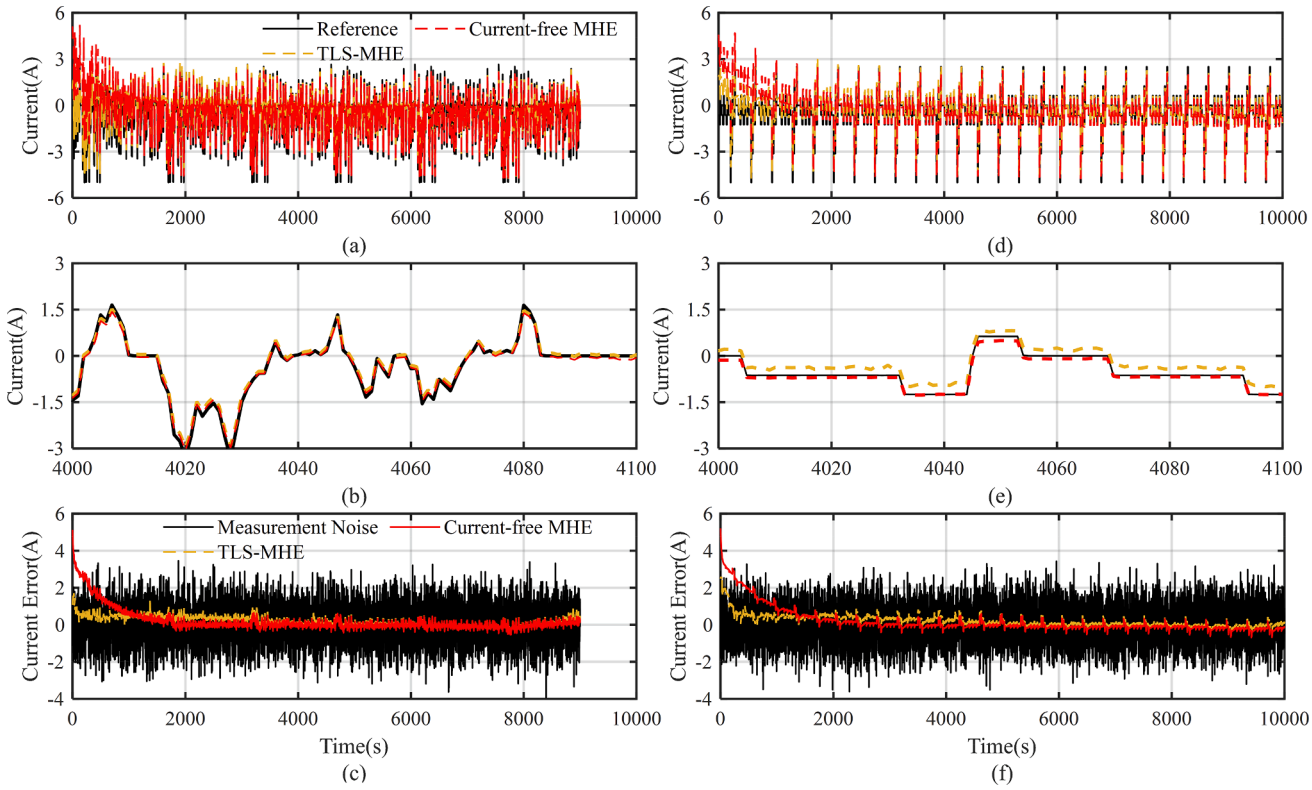

Fig. 11. Input current estimation results with heavy disturbances: (a-c) estimates and errors under FUDS, (d-f) estimates and errors under DST.

Table 6
Errors of input current estimate with heavy disturbances.

	FUDS		DST	
	MAE	RMSE	MAE	RMSE
TLS-MHE	0.244 A	0.314 A	0.231 A	0.305 A
Current-free MHE	0.135 A	0.191 A	0.161 A	0.208 A

The current estimation results by using the current-free MHE and the TLS-MHE are plotted comparatively in Fig. 11, and the statistical errors are summarized in Table. 5. The reported estimation accuracies show certain declinations compared with the foregoing given simulation results in Table 2. This is within expectation since the introduced model uncertainty inevitably discounts the performance of the discussed model-based estimator.

The overall performance of the current estimation is shown in Fig. 11 (a, d). Again, the convergence speed of the TLS-MHE is faster than the current-free MHE, which is consistent with the convergence of SOC estimation. As shown in Fig. 11 (b, e), the estimation accuracy of the current-free MHE is slightly higher than the TLS-MHE method after convergence, especially under the DST condition. Moreover, the estimation errors by using the two methods are both much smaller compared with the measurement noise, as illustrated in Fig. 11 (c, f), suggesting that the current measurement uncertainty has been mitigated to a large extent. Referring to Table. 6, the MAEs RMSEs of the current estimates are even smaller than the drifting error and the standard deviation of the random noises imposed on the current measurements.

Two major findings can be summarized from the experimental results in this section. First, the LS-MHE (Hierarchy I) is heavily biased and thus not applicable in the adverse condition of heavy noise corruption. Instead, both the TLS-MHE (Hierarchy II) and the current-free MHE (Hierarchy III) promise disturbance-immune performance. Second, in the even worse condition of no available current sensor, only the current-free MHE (Hierarchy III) can promise an accurate estimation of SOC. Moreover, the highly-authentic estimation of input current reported by current-free MHE also inspires the possibility to extend its practical use for the design of the virtual current sensor and the real-time current sensor fault diagnostic of the battery system.

5.5. Discussion on the practical application

Although the proposed method is designed to be implemented on a cell-level processor toward the future application of self-regulated smart batteries, it is also applicable to the conventional configuration of battery system. Particularly, the proposed method can be compiled into the BMS in advance. Considering the condition where both the voltage and current are measurable (e.g. in series branches), the Hierarchy II of the proposed method is activated, which can give an accurate SOC estimation using the noise-corrupted measurements. Considering the condition where the current is unmeasurable (e.g. in parallel branches or with failed current sensors), the Hierarchy III of the proposed method is activated, which can realize accurate co-estimation of both the SOC and input current. In the future, this endeavor can potentially contribute to reducing the expense of battery system by discarding the physical current sensors.

An undesirable effect is the growing computational burden when estimating the SOC and input current of all cells simultaneously. There can be two potential solutions to mitigate this adverse effect. First, each battery module can be equipped with one or more slave controllers to separate the huge computational burden into several affordable portions. Second, as depicted in BATTERY 2030 + Roadmap of Europe, higher degree of intelligent management is expected for the future battery system [42]. Within this vision, the system-level management can be realized in a distributed fashion by developing the self-regulated smart battery, which is generally devised with switches, sensors, and build-in cell-level processor. This endeavor will be focused on in our future work.

6. Conclusions

This paper proposes a hierarchical framework for the accurate soft measurement of battery SOC and load current. Within the proposed framework, three constrained optimization problems are formulated accounting for different degrees of current sensor uncertainties, and three estimation methods named LS-MHE, TLS-MHE and current-free MHE are developed by solving them in a real-time fashion. The primary conclusions are:

1. Under the scenario with accurate current measurements, the LS-MHE (Hierarchy I) is the best candidate with high accuracy and fast convergence. The MAEs of SOC estimation are 0.89% and 1.09% respectively under the FUDS and DST conditions.
2. Under the scenario of heavily-corrupted current measurement, both TLS-MHE (Hierarchy II) and current-free MHE (Hierarchy III) can provide accurate SOC estimate. The MAEs of SOC estimation with TLS-MHE (1.59% and 1.99%) and current-free MHE (0.87% and 1.67%) validate to be much smaller than those of LS-MHE (6.22% and 6.97%), under the FUDS and DST conditions.
3. Under the scenario of no current measurement, only the current-free MHE (Hierarchy III) is applicable for SOC estimation. The MAEs of the SOC estimation are as low as 0.78% and 1.45% respectively under FUDS and DST conditions.
4. The current-free MHE (Hierarchy III) can be used for the soft measurement of battery current. The normalized RMSEs of current estimation are smaller than 4%, which is in the same level with the widely-used Hall-effect current sensors. This unique merit inspires the possibility to extend its practical use for the design of virtual current sensor and the real-time current sensor fault diagnostic.

CRediT authorship contribution statement

Zhongbao Wei: Conceptualization, Methodology, Writing – original draft, Supervision, Funding acquisition. **Jian Hu:** Writing – review & editing, Methodology, Formal analysis, Investigation, Validation. **Yang Li:** Writing – review & editing, Methodology, Investigation. **Hongwen He:** Writing – review & editing, Resources. **Weihan Li:** Writing – review & editing. **Dirk Uwe Sauer:** Writing – review & editing.

Declaration of Competing Interest

The authors declare that they have no known competing financial interests or personal relationships that could have appeared to influence the work reported in this paper.

Acknowledgement

We would like to express our deep gratitude to the committee of the 12th International Conference on Applied Energy. We also gratitude the session chairs for their useful suggestions. This work is supported by the National Natural Science Foundation of China under Grant 52072038.

References

[1] Dong G, Yang F, Wei Z, Wei J, Tsui K-L. Data-driven battery health prognosis using adaptive Brownian motion model. IEEE Trans Ind Inf 2020;16(7):4736–46.
[2] Zheng Y, Ouyang M, Han X, Lu L, Li J. Investigating the error sources of the online state of charge estimation methods for lithium-ion batteries in electric vehicles. J Power Sources 2018;377:161–88.
[3] Ahmed MS, Raihan SA, Balasingam B. A scaling approach for improved state of charge representation in rechargeable batteries. Appl Energy 2020;267:114880. https://doi.org/10.1016/j.apenergy.2020.114880.
[4] Zhang C, Wang LY, Li X, Chen W, Yin GG, Jiang J. Robust and Adaptive Estimation of State of Charge for Lithium-Ion Batteries. IEEE Trans Ind Electron 2015;62(8):4948–57.
[5] Hu L, Hu X, Che Y, Feng F, Lin X, Zhang Z. Reliable state of charge estimation of battery packs using fuzzy adaptive federated filtering. Appl Energy 2020;262:114569. https://doi.org/10.1016/j.apenergy.2020.114569.
[6] Wei Z, Hu J, He H, Li Y, Xiong B. Load Current and State of Charge Co-Estimation for Current Sensor-Free Lithium-ion Battery. IEEE Trans Power Electron 2021;36(10):10970–5.
[7] Ziegler S, Woodward RC, Iu H-C, Borle LJ. Current Sensing Techniques: A Review. IEEE Sens J 2009;9(4):354–76.
[8] Souri K, Chae Y, Makinwa K. A CMOS temperature sensor with a voltage-calibrated inaccuracy of ±0.15°C (3σ) from −55 to 125°C. In: 2012 IEEE International Solid-State Circuits Conference; 2012. p. 208–10.
[9] Li Y, Wei Z, Xiong B, Vilathgamuwa DM. Adaptive Ensemble-Based Electrochemical-Thermal-Degradation State Estimation of Lithium-Ion Batteries. IEEE Trans Ind Electron 2021.
[10] Li Y, Xiong B, Vilathgamuwa DM, Wei Z, Xie C, Zou C. Constrained Ensemble Kalman Filter for Distributed Electrochemical State Estimation of Lithium-Ion Batteries. IEEE Trans Ind Inf 2021;17(1):240–50.
[11] Zou C, Hu X, Wei Z, Wik T, Egardt Bo. Electrochemical estimation and control for lithium-ion battery health-aware fast charging. IEEE Trans Ind Electron 2018;65(8):6635–45.
[12] Tian Y, Lai R, Li X, Xiang L, Tian J. A combined method for state-of-charge estimation for lithium-ion batteries using a long short-term memory network and an adaptive cubature Kalman filter. Appl Energy 2020;265:114789. https://doi.org/10.1016/j.apenergy.2020.114789.
[13] Wei Z, Zhao J, Ji D, Tseng KJ. A multi-timescale estimator for battery state of charge and capacity dual estimation based on an online identified model. Appl Energy 2017;204:1264–74.
[14] Zhu R, Duan B, Zhang J, Zhang Qi, Zhang C. Co-estimation of model parameters and state-of-charge for lithium-ion batteries with recursive restricted total least squares and unscented Kalman filter. Appl Energy 2020;277:115494. https://doi.org/10.1016/j.apenergy.2020.115494.
[15] Bian X, Wei Z, He J, Yan F, Liu L. A two-step parameter optimization method for low-order model-based state of charge estimation. IEEE Trans Transp Electrif 2021;7(2):399–409.
[16] Dai H, Wei X, Sun Z, Wang J, Gu W. Online cell SOC estimation of Li-ion battery packs using a dual time-scale Kalman filtering for EV applications. Appl Energy 2012;95:227–37.
[17] Wang Y, Zhang C, Chen Z. A method for state-of-charge estimation of LiFePO4 batteries at dynamic currents and temperatures using particle filter. J Power Sources 2015;279:306–11.
[18] Wang Y, Zhang C, Chen Z. On-line battery state-of-charge estimation based on an integrated estimator. Appl Energy 2017;185:2026–32.
[19] Ye M, Guo H, Cao B. A model-based adaptive state of charge estimator for a lithium-ion battery using an improved adaptive particle filter. Appl Energy 2017;190:740–8.
[20] Shu X, Li G, Shen J, Yan W, Chen Z, Liu Y. An adaptive fusion estimation algorithm for state of charge of lithium-ion batteries considering wide operating temperature and degradation. J Power Sources 2020;462:228132. https://doi.org/10.1016/j.jpowsour.2020.228132.
[21] Tang X, Gao F, Zou C, Yao Ke, Hu W, Wik T. Load-responsive model switching estimation for state of charge of lithium-ion batteries. Appl Energy 2019;238:423–34.
[22] Xiong B, Zhao J, Su Y, Wei Z, Skyllas-Kazacos M. State of charge estimation of vanadium redox flow battery based on sliding mode observer and dynamic model including capacity fading factor. IEEE Trans Sustainable Energy 2017;8(4):1658–67.
[23] Tang X, Wang Y, Chen Z. A method for state-of-charge estimation of LiFePO4 batteries based on a dual-circuit state observer. J Power Sources 2015;296:23–9.
[24] Hu X, Jiang H, Feng F, Liu Bo. An enhanced multi-state estimation hierarchy for advanced lithium-ion battery management. Appl Energy 2020;257:114019. https://doi.org/10.1016/j.apenergy.2019.114019.
[25] Hu X, Cao D, Egardt Bo. Condition Monitoring in Advanced Battery Management Systems: Moving Horizon Estimation Using a Reduced Electrochemical Model. IEEE/ASME Trans Mechatron 2018;23(1):167–78.
[26] Shen J-N, Shen J-J, He Y-J, Ma Z-F. Accurate State of Charge Estimation With Model Mismatch for Li-Ion Batteries: A Joint Moving Horizon Estimation Approach. IEEE Trans Power Electron 2019;34(5):4329–42.
[27] Lin X. Theoretical Analysis of Battery SOC Estimation Errors Under Sensor Bias and Variance. IEEE Trans Ind Electron 2018;65(9):7138–48.
[28] Zhang Z-L, Cheng X, Lu Z-Y, Gu D-J. SOC estimation of lithium-ion batteries with AEKF and wavelet transform matrix. IEEE Trans Power Electron 2017;32(10):7626–34.
[29] Kim J, Cho B. Application of wavelet transform-based discharging/charging voltage signal denoising for advanced data-driven SOC estimator. In Applied Power Electronics Conference and Exposition (APEC), 2015 IEEE. IEEE; 2015, p. 3013–8.
[30] Jiang Bo, Dai H, Wei X, Xu T. Joint estimation of lithium-ion battery state of charge and capacity within an adaptive variable multi-timescale framework considering current measurement offset. Appl Energy 2019;253:113619. https://doi.org/10.1016/j.apenergy.2019.113619.
[31] Putra WS, Dewangga BR, Cahyadi A, Wahyunggoro O. Current estimation using Thevenin battery model. In: Proceedings of the Joint International Conference on Electric Vehicular Technology and Industrial, Mechanical, Electrical and Chemical Engineering (ICEVT & IMECE). IEEE; 2015. p. 5–9.
[32] Dewangga BR, Herdjunanto S, Cahyadi A. Battery current estimation based on simple model with parameter update strategy using piecewise linear soc-ocv. In:

2018 4th International Conference on Science and Technology (ICST). IEEE; 2018. p. 1–6.
[33] Chun CY, Baek J, Seo G-S, Cho BH, Kim J, Chang IK, et al. Current sensor-less state-of-charge estimation algorithm for lithium-ion batteries utilizing filtered terminal voltage. J Power Sources 2015;273:255–63.
[34] Cambron DC, Cramer AM. A lithium-ion battery current estimation technique using an unknown input observer. IEEE Trans Veh Technol 2017;66(8):6707–14.
[35] Wang Y, Tian J, Sun Z, Wang Li, Xu R, Li M, et al. A comprehensive review of battery modeling and state estimation approaches for advanced battery management systems. Renew Sustain Energy Rev 2020;131:110015. https://doi.org/10.1016/j.rser.2020.110015.
[36] Wei Z, Dong G, Zhang X, Pou J, Quan Z, He H. Noise-Immune Model Identification and State-of-Charge Estimation for Lithium-Ion Battery Using Bilinear Parameterization. IEEE Trans Ind Electron 2021;68(1):312–23.
[37] Wei Z, Zhao D, He H, Cao W, Dong G. A noise-tolerant model parameterization method for lithium-ion battery management system. Appl Energy 2020;268:114932. https://doi.org/10.1016/j.apenergy.2020.114932.
[38] Haseltine E, Rawlings J. Critical Evalation of Extended Kalman Filtering and Moving-Horizon Estimation. Ind Eng Chem Res 2005;44:2451–60.
[39] Rao CV, Rawlings JB, Lee JH. Constrained Linear State Estimation—A Moving Horizon Approach. Automatica. 2001;37(10):1619–28.
[40] Grover MA, Rentian Xiong. A Modified Moving Horizon Estimator for In Situ Sensing of a Chemical Vapor Deposition Process. IEEE Trans Control Syst Technol 2009;17(5):1228–35.
[41] Shivappriya SN, Karthikeyan S, Prabu S, Pérez de Prado RPd, Parameshachari BD. A Modified ABC-SQP-Based Combined Approach for the Optimization of a Parallel Hybrid Electric Vehicle. Energies. 2020;13(17):4529. https://doi.org/10.3390/en13174529.
[42] Wei Z, Zhao J, He H, Ding G, Cui H, Liu L. Future smart battery and management: Advanced sensing from external to embedded multi-dimensional measurement. J Power Sources 2021;489:229462. https://doi.org/10.1016/j.jpowsour.2021.229462.